Rough-Wall Turbulent Heat Transfer Experiments in Hypersonic Free Flight

Michael C. Wilder*
NASA-Ames Research Center, Moffett Field, CA 94035-1000

and

Dinesh K. Prabhu †
Analytical Mechanics Associates, Inc., Moffett Field, CA 94035-1000

Rough-wall turbulent heat transfer measurements were obtained on ballistic-range models in hypersonic flight in the NASA Ames Hypervelocity Free Flight Aerodynamic Facility. Each model had three different surface textures on segments of the conic frustum: smooth wall, sand roughness, and a pattern roughness, thus providing smooth-wall and sand-roughness reference data for each test. The pattern roughness was representative of a woven thermal protection system material developed by NASA's Heatshield for Extreme Entry Environment Technology project. The tests were conducted at launch speeds of 3.2 km/s in air at 0.15 atm. Roughness Reynolds numbers, k^+, ranged for 12 to 70 for the sand roughness, and as high as 200 for the pattern roughness. Boundary-layer parameters required for calculating k^+ were evaluated using computational fluid dynamics simulations. The effects of pattern roughness are generally characterized by an equivalent sand roughness determined with a correlation developed from experimental data obtained on specifically-designed roughness patterns that do not necessarily resemble real TPS materials. Two sand roughness correlations were examined: Dirling and van Rij, et al. Both gave good agreement with the measured heat-flux augmentation for the two larger pattern roughness heights tested, but not for the smallest height tested. It has yet to be determined whether this difference is due to limitations in the experimental approach, or due to limits in the correlations used. Future experiments are planned that will include roughness patterns more like those used in developing the equivalent sand roughness correlations.

Nomenclature

h_w = enthalpy at the wall
H_0 = total enthalpy
k = roughness element height, or mean roughness height
k_s = equivalent sand grain roughness element height
k^+ = turbulent roughness Reynolds number, $\rho_w u_{\tau_0} k/\mu_w$
P = test section pressure
q = convective heat transfer rate
R_n = model nose cap radius
s = distance along surface from apex
S_a = arithmetical mean height of a surface
S_q = root mean square height of a surface
St = Stanton number, $q/(\rho_\infty u_\infty (H_0 - h_w))$
T = temperature
V_0 = launch velocity

* Aerospace Engineer, Aerothermodynamics Branch, MS 230-2; Associate Fellow, AIAA.
† Principal Research Scientist, Entry Systems and Technology Division, MS 229-1; Associate Fellow, AIAA.

$\bar{V}$ = average velocity
u_{τ_0} = smooth-wall friction velocity, $(\tau_w/\rho_w)^{1/2}$
α_{RMS} = root sum square of the total angle of attack
δ = boundary layer thickness
δ_s = laminar (or viscus) sublayer thickness
θ = momentum layer thickness
μ = fluid viscosity
ν = kinematic viscosity, μ/ρ
ρ = fluid density
σ = standard deviation
τ_w = surface shear stress

Subscripts
k = at the mean roughness height
r = on rough surface
s = on smooth surface
w = at the wall
0, stag = at stagnation point
∞ = at the free stream conditions

I. Introduction

The Heatshield for Extreme Entry Environment Technology (HEEET) project is developing a class of woven thermal protection system (TPS) materials as sustainable alternatives to carbon phenolic. The HEEET technology also provides the capability to tailor the material to a given entry mission in order to improve payload mass efficiency by altering the weave material, weave density, and resin.[1-4] An important consideration for any ablative TPS design is the effect of surface roughness on the atmospheric gases flowing over the vehicle during entry. Surface roughness can promote early boundary-layer transition and can significantly increase turbulent convective heat transfer[14, 18, 11-7] and skin friction[7, 8] above the smooth-wall values. The surface roughness initially formed on an ablating TPS material is characteristic of the composition and structure of the material. Composite materials such as chop-molded carbon phenolic, used for the Pioneer-Venus and Galileo missions, and Phenolic Impregnated Carbon Ablator (PICA), used for the Stardust sample return capsule shown in Fig. 1 (a),[5] form an irregular roughness much like densely-packed sand grains. In contrast, a woven TPS material, such as HEEET, forms a regular surface pattern determined by the weave architecture of the material, as shown in Fig. 1 (b).[6]

The effect of sand-grain roughness on the turbulent boundary layer heat transfer has been shown to correlate well with the ratio of the roughness height to the laminar sublayer thickness, as seen in Fig. 2, reproduced from Ref. 7, which shows the correlation of Powars to data obtained under the Passive Nosetip Technology (PANT) Program. This correlation defines an upper bound on heat-transfer augmentation. Other data sources have either been in agreement with this correlation, or measured lower levels of augmentation (for examples, see Refs. 8-12). As discussed in reviews by Bowersox[8] and Holden,[9] the lower augmentation seen in some data can be attributed to wall-temperature effects and/or effects of pressure-gradient and entropy swallowing, both of which are affected by the model geometry.

The shape and spacing of roughness elements on a woven-TPS surface can be markedly different from closely-packed, irregularly-shaped, sand grains. As a consequence, heat-transfer augmentation cannot be predicted with the correlation shown in Fig. 2 using only the roughness height. Schlichting[8] first proposed the use of an equivalent sand roughness, defined as the sand roughness size that produces the same effect on the boundary layer as a given pattern roughness. In this way, a semi-empirical correlation is used to account for shape and spacing of the roughness elements for an arbitrary pattern roughness. The available equivalent sand roughness correlations[13-18] were primarily developed from experimental data obtained on surfaces with regular patterns of two- and three-dimensional protuberances of simple geometrical shapes, such as sphere segments, cones, angles, or grooves, that do not necessarily resemble real TPS materials. A goal of the experiments reported here was to obtain turbulent heat transfer data on a pattern roughness representative of a woven TPS material for comparison with sand roughness data obtained during the same tests.

Rough-wall turbulent heat transfer measurements were obtained on ballistic-range models in hypersonic flight. Each model had three different surface textures on segments of the conic frustum: smooth wall, sand roughness, and a pattern roughness representative of a woven thermal protection system material. The pattern roughness was based on a 3D woven TPS material of the HEEET project. The models were 45° sphere-cones having a nose radius equal to

half the base radius. In terms of the pattern roughness spacing relative to the model base diameter, the models are a 4% geometrical scaling of a 0.76 m diameter full-size entry vehicle. Three roughness element heights were tested for the pattern roughness, representing virgin HEEET material, HEEET that has been ablated under turbulent shear-flow conditions, and a value twice the roughness of turbulent-ablated HEEET. The test condition was selected to produce boundary-layer scaling and convective heat transfer rates comparable to those computed for a Uranus atmospheric entry probe study reported in Ref. 19, and was used in previous sand-roughness experiments in the Ames ballistic range.[11] Equivalent sand roughness sizes were determined for the pattern roughness using the correlation of Dirling[14], which has been routinely applied in hypersonic and supersonic testing,[8-10, 12] and that of van Rij, *et al*.,[17] which is an extension of Sigal and Danberg[16] to allow evaluating 3D patterns of roughness having irregular geometry and arrangement more representative of real surfaces.

II. Experimental Approach

A. Ballistic-Range Models and Roughness Patterns

The model geometry was a 45° sphere-cone based on the fore-body geometry flown by the Galileo and Pioneer Venus missions. The models were made of titanium alloy Ti-6Al-4V with a nose radius of 7.62 mm (0.3 inch), a base diameter of 30.48 mm (1.2 in), and a shoulder radius of 0.762 mm (0.03 in), as sketched in Fig. 3 (a). Each model had three surface finishes on the frustum (smooth, sand roughness, and pattern roughness) arranged as shown in Fig. 3 (b). The two sand-roughness segments of the frustum provided reference measurements for evaluating the equivalent sand grain roughness for each pattern roughness tested. Sand roughness also covered the sphere-segment nose cap of each model to trip the boundary layer. The nose roughness was sized to achieve transition ahead of the sonic line for this test condition. Sand roughness was produced by the grit-blasting technique used in Ref. 11, and is assumed to produce textures similar to the grit-blasted surfaces used in developing Powars' correlation shown in Fig. 2.[7] Each model also had three smooth segments to provide a smooth-wall turbulent heating reference on each shot. The smooth areas had a measured arithmetical mean height, $S_a \leq 0.2$ μm, as determined from areal measurements made from confocal microscopy scans. The machine tool marks visible on the smooth surface areas in Fig. 3 (b) resulted in a slightly wavy wall, with an amplitude less than 1 μm ($k/\delta < 0.01$, $k/\delta_s < 0.3$) and a wavelength around 0.2 mm, which made no measurable impact on the heat transfer.

The pattern roughness was machined using a femtosecond laser ablation process[20] that removes material without significantly heating the surrounding material, thus reducing possible alterations to the material properties. The pattern was based on the HEEET 3D woven TPS material. A sample of HEEET[21] that was ablated in an arcjet under turbulent shear-flow conditions is shown in Fig. 4 (a). Also shown, Fig. 4 (b-d), are a close-up photograph of the surface texture, and elevation maps obtained from a 3D laser scan of the post-test surface that illustrate the basic weave pattern. Figure 5 details the idealized pattern roughness used for the ballistic range experiments. Figure 5 (a) and (b) show the basic pattern. Three roughness-element heights (nominally 10, 20, and 40 μm) were tested in the ballistic range, all having this roughness element distribution. Axial and diagonal height profiles for the three element heights are shown in Fig. 5 (c) and (d), respectively.

The element spacing on the ballistic range model, relative to the model base diameter, is 4% scale of the HEEET material on a 0.76 m diameter entry vehicle that was the subject of a Uranus mission study in Ref. 19. The model pattern with a 10 μm peak-to-valley roughness height represents the virgin HEEET surface roughness, and the 20 μm roughness height represents the nominal turbulent ablated HEEET surface roughness. Scans of the virgin and ablated HEEET surfaces are qualitatively compared with as-built 10, and 20 μm model surfaces in Fig.6. A third model roughness, with a nominal 40 μm roughness height, was also tested to provide an extreme case having a (scaled) roughness height slightly larger than heritage carbon phenolic.[22] Figure 7 shows portions of scans of representatives of all three pattern roughness heights, as well as of three of the sand roughened surfaces produced. The grit-blasting technique currently in use is not capable of producing roughness greater than ~20 μm.

Each surface was characterized using data from confocal microscopy scans of areas located near the mid-frustum, which were analyzed using in-house-developed software that identifies individual roughness elements and calculates the roughness height statistics. The scan area was approximately 2.8 mm axial ($\Delta s/R_n \sim 0.37$) x 1.4 mm circumferential, which contained approximately 850 roughness elements for the pattern roughness. For a subset of models additional scans were obtained at other areas to verify uniformity of the surface texture. Roughness element height distributions are plotted in Fig. 8 for the six representative surfaces shown in Fig. 7.

B. Facility and Techniques

The experiments were performed in the Hypervelocity Free Flight Aerodynamic Facility (HFFAF) ballistic range at NASA Ames Research Center.[23] The facility has a suite of guns for launching model entry vehicles through a 23 m long enclosed test section. These tests employed a two-stage light-gas gun with an inner diameter of 38.1 mm (1.5 in). The test section, shown in Fig. 9, is approximately 1 m across and can be evacuated to pressures ≤ 1 atm, or can be back-filled with various test gases for simulating flight through other atmospheres.

The attitude and position of a model in flight are obtained from sixteen pairs of orthogonal shadowgraph images. The imaging stations are spaced 1.524 m (5 ft) apart, along the length of the test section. The shadowgraphs are spark-illuminated and Kerr-cell shuttered, giving a 40 ns exposure. High-speed counters activated by the Kerr-cells record the flight time between each station.

Heat transfer on the models was determined from instantaneous global surface temperature distributions recorded with three thermal imaging cameras, sensitive to the 3-5 μm infrared wavelength band. The cameras were placed at three locations along the flight path and arranged to provide a nearly head-on view of the model. An example shadowgraph and thermal image are shown in Fig. 10. Heat flux was determined from the measured surface temperatures, assuming one-dimensional conduction at the model surface and using the temperature-dependent thermo-physical properties of the material from which the models were fabricated. Measurement uncertainty is estimated to be ±15% (three standard deviations) based on the standard deviation of stagnation-point heat flux measurements averaged over numerous runs. This includes uncertainty due to run-to-run variations in test conditions, such as launch speed, but is mainly driven by uncertainties in the thermo-physical properties of the material, such as emissivity and thermal conductivity. Further details about the measurement and calibration techniques can be found in Refs. 23 and 24.

C. Test Conditions

The nominal test condition was a launch velocity of 3.22 km/s into room-temperature air at 0.15 atm pressure. This test condition was intended to match one of the conditions previously used to measure the rough-wall heat transfer on sand-roughened surfaces reported in Ref. 11, and was selected to produce boundary-layer scaling and convective heat transfer rates comparable to those computed for a Uranus atmospheric entry probe study reported in Ref. 19. The actual conditions for each shot are given is Table 1. Mach and Reynolds numbers are based on the launch velocity, V_0. Uncontrollable perturbations to the model during launch result in angle of attack oscillations in flight. For the tests reported here the models executed approximately three oscillation cycles over the length of the test section, and typical angles, represented as the root-mean-square (RMS) of the total angle of attack, were less than 3 degrees. Unusually large angle oscillations were observed for shot 2808, which were due to an impact by a piece of sabot debris on the base of the model. The measured heat-flux distribution on this model showed no unusual asymmetries due to the oscillations. Heat flux on the frustum was slightly lower than for other shots, however, the ratio of rough-wall to smooth-wall heat flux was in agreement with results from a repeat shot (2809), therefore, the results are reported here. Sand roughness on the sphere-segment nose cap was used to trip the flow. The nose surface of each model was scanned over a 1.5 x 1.5 mm^2 area and the mean roughness height, k_n, and the standard deviation of roughness heights are given for each model in Table 1. The stagnation temperature reported in Table 1 was measured at the mid-range location in the test section. The stagnation heat flux in Table 1 is the cold-wall heat flux, which is the heat flux at the launch condition determined from the measurements.

Table 2 provides measurements on the smooth-wall section of each model at $s/R_n = 1.7$, midway along the frustum. The wall temperature, T_w, and heat flux values, q_s, were averaged over an area spanning $1.55 \le s/R_n \le 1.85$, and 20^o circumferentially. The average standard deviation of q_s over this area was less than 0.5%. The tabulated values were obtained at the center of the large (120^o) smooth segment shown in Fig. 3 (b), but comparable results were obtained in the two narrower smooth segments. The parameter u_{τ_0}/ν_w was computed for each shot, as described in the next section, and was used to calculate the roughness Reynolds number, $k^+ = u_{\tau_0}k/\nu_w$, for each shot, as described in the results section. The smooth-wall surface finish was not measured for all models. Where values are provided, the surface was scanned over an area 2.8 mm long (axial), and 0.8 mm wide (circumferential).

Table 1. Test Conditions

Shot	V_0, km/s	M_0	Re_D	$\bar{V}$, km/s	P_∞, N/m^2	ρ_∞, kg/m^3	T_∞, K	α_{RMS}, deg	k_n, μm	$\sigma(k_n)$	T_{stag}, K	q_{stag}, W/cm^2
2805	3.27	9.49	9.69E+05	2.99	15185.4	0.1796	294.6	2.5	15.8	4.1	806.3	3239
2807	3.33	9.68	9.88E+05	3.06	15198.8	0.1795	295.0	2.3	19.2	2.9	828.5	3446
2808	3.23	9.39	9.60E+05	2.97	15212.1	0.1799	294.6	14.2	19.8	2.5	824.5	3357
2809	3.22	9.37	9.58E+05	2.97	15198.8	0.1798	294.5	2.0	20.1	4.0	854.9	3186
2810	3.26	9.49	9.75E+05	3.00	15198.8	0.1805	293.3	2.5	16.6	3.6	796.4	3177
2811	3.22	9.37	9.60E+05	2.95	15198.8	0.1801	293.9	2.6	15.6	3.4	852.8	3582
2812	3.12	9.09	9.31E+05	2.87	15198.8	0.1801	294.0	4.5	17.4	4.2	786.7	3008
2813	3.12	9.08	9.32E+05	2.87	15212.1	0.1805	293.6	2.8	16.2	4.5	779.8	2965

Table 2. Smooth-Wall Properties at Mid-Frustum, $s/R_n = 1.7$.

Shot	k, μm	σ(k)	k/δ	S_a, μm	S_q, μm	T_w, K	q_s, W/cm^2	u_{τ_0}/ν_w, (μm)$^{-1}$
2805	0.87	0.13	0.005	0.17	0.23	689.4	2349	3.58
2807	0.61	0.11	0.003	0.21	0.27	709.0	2509	3.46
2808						645.3	2022	3.88
2809	0.50	0.11	0.003	0.17	0.21	694.3	2095	3.55
2810						700.6	2437	3.51
2811						690.6	2335	3.57
2812						673.6	2190	3.68
2813						666.2	2132	3.73

D. Computational Approach

Computational fluid dynamics (CFD) solutions were generated using the Data Parallel Line Relaxation (DPLR) code[25] for an axisymmetric geometry. A 5-species chemically reacting model was employed for the test gas: N_2, O_2, NO, N, and O. In all computations thermal equilibrium (i.e., a single temperature) was assumed and thermodynamic properties (enthalpy and specific heat) of constituent species were determined using GRC curve fits.[26] All cases were computed with a prescribed wall temperature, given in Table 3, and the wall was assumed to be fully catalytic to recombination of atomic species (N and O). Turbulent-flow computations employed the simple algebraic turbulence model of Baldwin and Lomax,[27] which has been modified by Rizk[28] to handle surfaces with sand roughness, with the mean roughness height as a user-specified input. Boundary-layer parameters from the smooth-wall turbulent CFD solutions were used to calculate the roughness Reynolds number, $k^+ = u_{\tau_0} k/\nu_w$, for each test case. Table 3 lists the CFD cases and boundary-layer parameters for the nominal launch condition, and at the mid-range velocity for a range of wall temperatures. In order to determine the k^+ value for each rough surface tested, the computed smooth-wall u_{τ_0}/ν_w at the mid-range velocity was interpolated to the measured mid-range wall temperature (see Table 2), and multiplied by either the mean measured k, or the equivalent sand roughness, k_s, as appropriate.

Table 3. CFD Conditions and Smooth-Wall Turbulent Boundary-Layer Parameters.

V, km/s	P, atm	P, N/m^2	T_{gas}, K	T_w, K	θ, μm	δ, μm	δ_s, μm	u_{τ_0}/ν_w, (μm)$^{-1}$
3.222	0.15	15198.75	300	300	32.70	207.90	0.97	11.39
2.988	0.15	15198.75	300	300	31.88	201.89	1.13	9.74
				650	32.63	212.61	2.86	3.85
				750	32.60	213.76	3.39	3.25
				850	32.67	216.14	3.92	2.80
				950	32.61	217.14	4.47	2.46
				1050	32.47	217.44	5.04	2.18

III. Results and Discussion

Measured and computed laminar and turbulent smooth-wall heat flux profiles are shown in Fig. 11 (a). The laminar measurement, obtained on an entirely-smooth model, was performed in an earlier test campaign reported in Ref. 11. The error bars for that profile represent ±15% of the local heat flux. Since each shot in the current campaign had a smooth-wall segment it was possible to determine statistics on the turbulent-flow measurements. Recall that the nose cap ($s/R_n < 0.707$) was rough for the current shots in order to trip the flow to turbulence. The roughness height for each shot was given in Table 1. The turbulent measurement result in Fig. 11 (a) shows the eight-shot average profile, with the error bars representing three standard deviations. The average standard deviation along the mean profile was 5.1%, showing good repeatability. The models in the current test campaign were supported for launch differently than the model for the laminar measurement, which may account for the drop in heat flux near the shoulder ($s/R_n > 2.2$) in the turbulent measurements. The roughness augmentation results were all taken upstream of this region.

For each shot, the rough-wall profiles were divided by the smooth-wall profile from the same shot, q_r/q_s, which is equivalent to the Stanton number ratio, St_r/St_s, since the wall enthalpy is small relative to the total enthalpy, $H_0 = V^2/2$. All profile data were averaged over 20° circumferentially around the cone, and centered in the specified texture segment of the model (refer to Fig. 3 (b) for the segment layout). Figure 11 (b) shows the rough-to-smooth ratio profiles on the frusta for representative shots of the three pattern roughness heights, and two sand roughness heights. Also shown are the rough-wall CFD results. It can be seen that q_r/q_s is relatively flat along the frustum. The rough-wall CFD for k = 10 and 20 μm are in good agreement with the sand-roughness measurements. There were no measurements with larger sand roughness heights.

Heat-flux augmentation factors were determined by averaging over a length centered on the mid-frustum, $1.55 \le s/R_n \le 1.85$, as indicated in Fig. 11 (b). Tables 4 and 5 give the roughness Reynolds numbers, k^+, and heat-flux augmentation factors, q_r/q_s, for each shot, for the pattern and sand roughness, respectively. For the pattern roughness, k^+ in Table 4 is based on the actual mean roughness element height, rather than the more-common equivalent sand roughness height, k_s, as discussed below. The tables are arranged in order of increasing k, rather than by shot number. The roughness Reynolds numbers, k^+, are the product of the measured k and the value of smooth-wall u_{τ_0}/ν_w interpolated from the computed values in Table 3 to the measured smooth-wall temperatures in Table 2 for each shot. The tables also give the augmentation factor predicted by the Powars' correlation, previously shown in Fig. 2, and the percent difference of the measured augmentation relative to the predicted values. It can be seen that all are within the uncertainty band of the original PANT data, shown in Fig. 2. Finally, Table 5 gives two data points for each shot, corresponding to the two sand-roughness panels on each model (see again Fig. 3 (b)). Roughness heights were not measured on the second sand-roughness section for every model. In those cases, the measured k from the first area was used for both. Where both areas were measured, the mean roughness heights differed by less than one standard deviation.

The augmentation factors are plotted in Fig. 12 against the Powars correlation. Also plotted are the previously-obtained sand-roughness measurements from Ref. 11, and the rough-wall CFD results for k = 10, 20, and 40 μm. The CFD results were evaluated for the T_w = 650 K case at the mid-range velocity, which is closest to the average mid-range wall temperature. Error bars are only shown on the pattern-roughness results to avoid clutter. The vertical error bars are three times the uncertainty on q_r/q_s as determined from the standard variance formula for the propagation of error,[29] where the uncertainty on each heat-flux term is equal to the 5.1% standard deviation of the shot-to-shot variation. This gives an uncertainty of the heat-flux ratio of $w(q_r/q_s) \sim 8.7\%$, and $3w \sim 26\%$ for the error bars. In the course of the ballistic-range model's flight, the k^+ value will vary as the wall viscosity changes with the model's wall temperature. The horizontal error bars are the root-sum-square error of the amount k^+ changes due to wall temperature changes between the first and last measurement stations (which is the primary contributor), and the uncertainty in measured k, represented as three standard deviations from the measured mean k.

Table 4. Roughness Reynolds Numbers and Augmentation Factors for Pattern Roughness

Shot	k, μm	σ(k), μm	k/δ	T_w, K	q_r, W/cm^2	k^+	q_r/q_s (Measured)	q_r/q_s (Powars)	% diff q_r/q_s (meas. – Powars)
2809	10.2	0.2	0.05	792.7	2742	36	1.31	1.37	-5%
2808	10.5	0.2	0.05	739.4	2698	41	1.33	1.41	-5%
2812	10.5	0.3	0.05	740.5	2663	39	1.22	1.39	-13%
2813	18.8	0.5	0.09	787.6	3015	70	1.41	1.56	-10%
2811	19.1	0.2	0.09	817.9	3312	68	1.42	1.56	-9%
2810	19.7	0.3	0.09	838.7	3516	69	1.44	1.56	-8%
2805	39.5	0.5	0.18	901.7	4042	141	1.72	1.77	-3%
2807	42.6	0.5	0.20	933.1	4356	148	1.74	1.78	-2%

Table 5. Roughness Reynolds Numbers and Augmentation Factors for Sand Roughness

Shot	k, μm	σ(k), μm	k/δ	T_w, K	q_r, W/cm^2	k^+	q_r/q_s (Measured)	q_r/q_s (Powars)	% diff q_r/q_s (meas. – Powars)
2805	3.7	0.5	0.02	737.1	2702	13	1.15	1.08	6%
2805	3.4	0.5	0.02	734.5	2679	12	1.14	1.05	8%
2812	4.6	0.6	0.02	713.2	2464	17	1.13	1.15	-2%
2812	4.9	0.6	0.02	709.0	2432	18	1.11	1.17	-5%
2808	5.1	0.7	0.02	693.0	2351	20	1.16	1.20	-3%
2808				696.3	2378	20	1.18	1.20	-2%
2811	7.8	1.2	0.04	770.3	2934	28	1.26	1.30	-3%
2811				763.4	2884	28	1.24	1.30	-5%
2809	8.5	1.0	0.04	811.5	2875	30	1.37	1.32	4%
2809				836.7	3057	30	1.46	1.32	11%
2813	11.4	1.8	0.05	778.0	2952	42	1.38	1.42	-2%
2813	12.2	1.5	0.06	764.0	2852	46	1.34	1.44	-7%
2807	16.1	3.0	0.07	888.0	3955	56	1.58	1.50	5%
2807	16.0	3.8	0.07	895.8	4022	55	1.60	1.50	7%
2810	20.2	2.9	0.09	900.9	4040	71	1.66	1.57	6%
2810				895.8	3993	71	1.64	1.57	5%

It is clear from Fig. 11 (b) that the pattern roughness of a given k resulted in less heat-transfer augmentation than sand roughness of a comparable mean roughness height. Even so, the measured augmentation is in good agreement with the Powars correlation when evaluating the roughness Reynolds number based on the mean roughness element height, k, as seen in Fig. 12 and Table 4. The lower augmentation relative to sand roughness was expected, since the roughness elements are less densely packed than for sand roughness, and the element shapes are smoother than sand. In the study of rough-wall effects, pattern roughness is typically characterized by an equivalent sand roughness, k_s, defined as the sand roughness height that produces the same effect as the given pattern roughness. The effect of the pattern roughness is correlated to the effect of sand roughness from experimental data using some form of shape parameter that depends on the pattern roughness density relative to the roughness element height, and, usually, some form of bluntness factor related to the shape of the roughness elements. There are a number of equivalent sand roughness correlations in the literature (Refs. 13-18, for examples), but the correlation of Dirling[14] has frequently been employed for interpreting hypersonic test results.[8-10, 12] An extension of Schlichting's[13] experiments for roughness elements consisting of hemispheres, sphere segments, cones, and right angles at various spacings, Dirling accounts for the roughness element bluntness, as well as for the element density. Most data in the literature have been obtained on Schlichting-like patterns, which consist of protuberances on an otherwise (locally) flat surface that are arranged such that elements are equidistantly spaced in all directions. In contrast, the woven TPS patterns considered here have continuously-varying surface elevations (local valleys, rather than a local plane), and two spacing scales – axial and diagonal – as shown in Figs. 4 and 5. A more recent equivalent sand roughness correlation was proposed by van Rij, *et al.*,[17] which is an extension of Sigal and Danberg[16] to allow evaluating 3D patterns of roughness with irregular geometry and arrangement more representative of real surfaces.

The equivalent sand grain roughness height ratio, k_s/k, was evaluated for each pattern roughness using both the Dirling correlation and the van Rij correlation (refer to Refs. 14 and 17 for the details of the correlations). The Dirling correlating parameter includes a density parameter, D/k, where D is defined as the inverse square root of the number of roughness elements per unit geometric surface area. The Dirling correlation was evaluated in two ways: 1) using the above definition of D, which gives D ≅ 79 μm, which also equals the average roughness element diameter identified by our surface analysis software; 2) using D = 50 μm, which is the peak-to-valley spacing (which is uniform in all directions), as well as the axial spacing between weave pattern rows and columns (refer again to Fig. 5). Results for each correlation are given in Table 6, and plotted in Fig. 13. For convenience, Table 6 also includes some data from Table 4: the measured k and augmentation factors (q_r/q_s), k^+ evaluated using k, and the percent difference of q_r/q_s relative to the value predicted using the Powars rough-wall correlation for k^+. This percent difference was also evaluated for each of the resulting k_s^+ values, and presented in Table 6. For the 20 μm pattern roughness, all three approaches yield a roughness Reynolds number, k_s^+, that is within the expected uncertainty of the Powars correlation for the measured heat-flux augmentation. For the 40 μm pattern roughness, this is true only for the second treatment of Dirling and the van Rij correlation. For the 10 μm roughness height, all three equivalent sand roughness heights indicate an aerodynamically smooth wall, $k_s^+ < 10$. It is not clear at the time of writing whether these correlations are suited for the woven TPS type roughness pattern at small roughness heights, or whether the heat-flux augmentation measurements are suspect (the measured augmentation was 20 to 30%, while the estimated uncertainty, as discussed above, is ~26%). Note, however, that sand-roughness measurements at low augmentation levels were in good agreement with the established trend, as seen in Fig. 12.

Table 6. Equivalent Sand Roughness and Roughness Reynolds Numbers.

Shot	k, μm	k^+	q_r/q_s	% diff q_r/q_s (meas. – Powars)	k_s/k			k_s^+			%diff q_r/q_s meas – Powars(k_s^+)		
					Dirling 1	Dirling 2	Van Rij	Dirling 1	Dirling 2	Van Rij	Dirling 1	Dirling 2	Van Rij
2809	10.2	36	1.31	-5%	0.05	0.10	0.19	2	3	7	31%	31%	31%
2808	10.5	41	1.33	-5%	0.05	0.10	0.18	2	3	7	33%	33%	33%
2812	10.5	39	1.22	-13%	0.05	0.10	0.20	2	3	8	22%	22%	22%
2813	18.8	70	1.41	-10%	0.49	0.89	1.00	34	51	70	4%	-4%	-10%
2811	19.1	68	1.42	-9%	0.51	0.92	1.03	35	52	71	4%	-4%	-9%
2810	19.7	69	1.44	-8%	0.57	1.04	1.15	40	59	80	3%	-5%	-10%
2805	39.5	141	1.72	-3%	6.73	2.04	1.94	951	210	274	-26%	-9%	-12%
2807	42.6	148	1.74	-2%	5.29	1.60	1.93	780	171	285	-23%	-5%	-12%

IV. Application to HEEET for Outer Planet Missions

Heat-transfer augmentation due to the surface roughness of the HEEET material shown in Fig. 4 will be considered for notional missions to Uranus and Saturn. The effect of transpiration cooling from ablation product blowing in not considered here. The entry trajectories were based on mission studies performed in support of the Planetary Science Decadal Survey.[30] The forebody of both probe vehicles employed a spherically-blunted 45° cone with a nose radius equal to half the base radius, similar to the ballistic-range models of the experiments reported here. The Saturn probe base diameter was 1.0 m, and the Uranus probe base diameter was 0.76 m. Smooth-wall CFD simulations were performed by Palmer, *et al*.[19] on several trajectory points for atmospheric entry at Saturn and Uranus. For the Saturn entry, peak heating occurred at 272 s after entry interface, and for the Uranus entry trajectory, peak heating occurred at 42.5 s. Further details regarding the trajectories and the computational methods can be found in Ref. 19.

The measured roughness parameters for the HEEET sample are given in Table 7 for virgin and ablated surfaces. As with the model pattern roughness in the previous section, an equivalent sand roughness was evaluated using both the Dirling and the van Rij correlations, and two methods of calculating the element density parameter were used for the Dirling correlation: 1) used the mean roughness element diameter, D, in Table 7; 2) used the mean peak-to-valley spacing, L, in Table 7. It is seen that the equivalent sand roughness for the virgin material is orders of magnitude smaller than the measured roughness size for all three methods, while for the ablated material it is between 0.5 and 1 times the actual height. Similar results were found for the 10 and 20 μm model pattern roughness (by design, since the models were based on this TPS material).

Table 8 gives the roughness Reynolds numbers for k and the various k_s values, and the heat-flux augmentation factors at the mid-frustum location calculated using Powars' correlation for each value of the roughness Reynolds number. Only values at the peak-heating trajectory points are shown because, at the other trajectory points computed for Ref. 19 the roughness Reynolds numbers never exceeded 10, the smooth-wall limit. Even at the peak-heating point,

the Saturn entry vehicle never exceeded a roughness Reynolds number of 10. The roughness Reynolds number and heat-flux augmentation factor profiles along the vehicles are plotted in Fig. 14 for these cases.

Table 7. Characterization of Example Woven TPS Roughness (Fig. 4).

Sample State	k, mm	σ(k), mm	D, mm (mean element diameter)	L, mm (mean peak-to-valley separation)	k_s/k		
					Dirling 1 (based on D)	Dirling 2 (based on L)	Van Rij
virgin	0.21	0.04	2.4	1.9	0.005	0.007	0.019
ablated	0.74	0.22	2.3	1.6	0.515	0.970	0.652

Table 8. Heat Transfer Augmentation due to Woven TPS Roughness on Example Missions.

Mission	TPS State	time, s	Mid-frustum q, W/cm^2	k^+	k_s^+			St_r/St_s predicted by Powars			
					Dirling 1	Dirling 2	van Rij	Based on k	Based on Dirling 1 k_s	Based on Dirling 2 k_s	Based on van Rij k_s
Uranus	virgin	42.5	1556	19.3	0.1	0.1	0.4	**1.19**	1	1	1
	ablated	42.5	1556	67.7	34.8	65.6	44.2	**1.55**	**1.36**	**1.54**	**1.43**
Saturn	ablated	272	609	7.4	3.8	7.2	4.8	1	1	1	1

V. Summary

It is well established that surface roughness can amplify turbulent-flow skin friction and heat transfer under the right conditions. Understanding how a TPS surface roughness will interact with the entry environment is necessary when designing TPS for a given mission. In the cases where the roughness elements form regular patterns, such as for woven materials, the roughness effects are typically accounted for by use of various semi-empirical correlations that characterize the surface roughness by a single value, the equivalent sand roughness height. The available equivalent sand roughness correlations have typically been developed from experimental data obtained on specifically-designed roughness patterns that do not necessarily resemble real TPS materials. The experiments reported here obtained turbulent heat transfer data on a pattern roughness representative of a woven TPS material for comparison with sand roughness data obtained during the same tests.

Rough-wall turbulent heat transfer measurements were obtained on ballistic-range models in hypersonic flight. Each model had three different surface textures on segments of the conic frustum: smooth wall, sand roughness, and a pattern roughness representative of a woven thermal protection system material. The pattern roughness was based on a new class of 3D woven TPS materials under development by NASA's Heatshield for Extreme Entry Environment Technology (HEEET) project. The models were 45° sphere-cones having a nose radius equal to half the base radius. In terms of the pattern roughness spacing relative to the model base diameter, the models are a 4% geometrical scaling of a 0.76 m diameter full-size entry vehicle. Three roughness element heights were tested for the pattern roughness, representing virgin HEEET material, HEEET that has been ablated under turbulent shear-flow conditions, and a value twice the roughness of turbulent-ablated HEEET. The test condition was selected to produce boundary-layer scaling and convective heat transfer rates comparable to those computed for a Uranus atmospheric entry probe study reported in Ref. 19. Heat transfer data on sand roughness were also obtained previously at this test condition (reported in Ref. 11) and compared well with the new data.

Equivalent sand roughness sizes were determined for the pattern roughness using two correlations in the literature: Dirling and van Rij. When defining the roughness element density for the Dirling correlation to be based on the row and column spacing of the elements (the equivalent of the yarn spacing for the woven TPS material) rather than the mean element spacing, the roughness Reynolds number based on the equivalent sand roughness height is in good agreement with the data for the larger two roughness sizes. For the smallest roughness, representing the virgin TPS material, the correlations indicate a functionally smooth surface (no heat-flux augmentation) for the tested conditions, while the experiments measured 20% to 30% augmentation. It has yet to be determined whether this difference is due to limitation in the experimental approach, or due to limits in the correlations used. Future experiments are planned that will include roughness patterns more like those used in developing the equivalent sand roughness correlations.

Acknowledgments

This work was supported by NASA's Entry Systems Modeling (ESM) Project. Dinesh K. Prabhu is supported by Space Technology Research and Development Contract NNA15BB15C from NASA Ames Research Center to Analytical Mechanics Associates, Inc. The authors wish to thank Charles Cornelison, Donald Bowling, Alfredo Perez, and Jon-Pierre (JP) Wiens for their support in conducting the experiments, Shawn Meszaros of NASA Ames for fabricating the sand grain roughness, and Matt Melonio of Providence Texture for producing the pattern roughness sections.

References

[1] Ellerby, D., *et al.*, "Overview of Heatshield for Extreme Entry Environment Technology (HEEET) Project," 15th International Planetary Probe Workshop; 9-15 June, 2018, Boulder, CO.

[2] Stackpoole, M., *et al.*, "Heatshield for Extreme Entry Environment Technology (HEEET) - Enabling Missions Beyond Heritage Carbon Phenolic," National Space and Missile Materials Symposium (NSMMS), 26-29 June, 2017.

[3] Venkatapathy, E., *et al.*, "TPS for Outer Planets," Outer Planets Assessment Group (OPAG) Technology Forum; 21-22 Feb. 2018, Hampton, VA.

[4] Mahzari, M. and Milos, F., "Sizing and Margin Methodology for Dual-Layer Thermal Protection Systems," 15th International Planetary Probe Workshop; 11-15 June 2018, Boulder, CO.

[5] Kontinos, D. A. and Stackpoole, M., "Post-Flight Analysis of the Stardust Sample Return Capsule Earth Entry," AIAA 2008-1197, 46th AIAA Aerospace Sciences Meeting and Exhibit, 7 - 10 January 2008.

[6] Milos, F. S., Chen, Y.-K., and Mahzari, M., "Arcjet Tests and Thermal Response Analysis for Dual-Layer Woven Carbon Phenolic," *Journal of Spacecraft and Rockets*, Vol. 55, No. 3, 2018, pp. 712-722.

[7] Wool, M. R., "Final Summary Report Passive Nosetip Technology (PANT) Program," Aerotherm Report 75-159, June 1975.

[8] Bowersox, R., "Survey of High-Speed Rough Wall Boundary Layers: Invited Presentation," AIAA 2007-3998, 37th AIAA Fluid Dynamics Conference, Miami, FL, 25 - 28 June 2007.

[9] Holden, M. S., et al., "A Review of Experimental Studies of Surface Roughness and Blowing on the Heat Transfer and Skin Friction to Nosetips and Slender Cones in High Mach Numbers Flows," AIAA 2008-3907, 40th Thermophysics Conference, June 2008.

[10] Hollis, B. R., "Distributed Roughness Effects on Blunt-Body Transition and Turbulent Heating," AIAA 2014-0238, 52nd AIAA Aerospace Sciences Meeting, 13-17 January 2014.

[11] Wilder, M. C., Reda, D. C., and Prabhu, D. K., "Effects of Distributed Surface Roughness on Turbulent Heat Transfer Augmentation Measured in Hypersonic Free Flight," AIAA-2014-0512, 52nd AIAA Aerospace Sciences Meeting, 13-17 January 2014.

[12] Neeb, D., Gülhan, A., and Merrifield, J. A., "Rough-Wall Heat Flux Augmentation Analysis within the ExoMars Project," *Journal of Spacecraft and Rockets*, Vol. 53, No. 1, 2016, pp. 121-133.

[13] Schlichting, H., "Experimental Investigation of the Problem of Surface Roughness," NACA Technical Memeorandum No. 823, April 1937.

[14] Dirling, R.B. Jr., "A Method for Computing Roughwall Heat Transfer Rates on Reentry Nosetips," AIAA 73-763, AIAA 8th Thermophysics Conference, Palm Springs, CA, July 1973.

[15] Simpson, R., "A Generalized Correlation of Roughness Density Effects on the Turbulent Boundary Layer," *AIAA Journal*, Vol. 11 No. 2, Feb. 1973, pp. 242-244.

[16] Sigal, A., and Danberg, J. E., ''New Correlation of Roughness Density Effect on the Turbulent Boundary Layer,'' *AIAA Journal*, Vol. 28, No. 3, 1990, pp. 554–556.

[17] van Rij, J. A., Belnap, B. J., and Ligrani., P. M., "Analysis and Experiments on Three-Dimensional, Irregular Surface Roughness," *Journal of Fluids Engineering*, Vol. 124, No. 3, 2002, pp. 671-677.Dirling, R.B. Jr., "On the relation between material variability and surface roughness," AIAA 1977-402, 18th Structural Dynamics and Materials Conference, March 1977.

[18] Finson, M. L. and Clarke, A. S., "The Effect of Surface Roughness Character on Turbulent Reentry Heating," AIAA 80-1459, AIAA 15th Thermophysics Conference, Snowmass, CO, July 1980.

[19] Palmer, G., Prabhu, D. K., and Cruden, B. A., "Uncertainty Determination for Aeroheating in Uranus and Saturn Probe Entries by the Monte Carlo Method," AIAA 2013-2776, 44th AIAA Thermophysics Conference, 24-27 June, 2013.

[20] Aizawa, T. and Inohara, T., "Pico- and Femtosecond Laser Micromachining for Surface Texturing," *Micromachining*, February, 2019 (DOI: http://dx.doi.org/10.5772/intechopen.83741).

[21] Venkatapathy, E., *et al.*, "Heatshield for Extreme Entry Environment Technology (HEEET)," 11th Venus Exploration Analysis Group (VEXAG) Meeting, Washington, DC, 19-21 Nov. 2013.

[22] Brewer, R., Wolfe, J., and Metzger J., "Utilization of a ground test facility to obtain verification of the full scale Pioneer Venus nosecap heat shield," AIAA 1977-0759, 12th Thermophysics Conference, June 1977.

[23] Wilder, M.C., Bogdanoff, D. W., and Cornelison, C. J., "Hypersonic Testing Capabilities at the NASA Ames Ballistic Ranges," AIAA 2015-3339, AIAA Aerospace Sciences Meeting, Kissimmee, Florida, 5-9 January 2015.

[24] Wilder, M.C., Reda, D.C., and Prabhu, D.K., "Heat-Transfer Measurements on Hemispheres in Hypersonic Flight through Air and CO_2," AIAA 2011-3476, 42nd AIAA Thermophysics Conference, 27 - 30 June 2011, Honolulu, Hawaii.

[25] Wright, M. J., White, T., and Mangini, N., "Data-Parallel Line Relaxation Methods (DPLR) Code User Manual Acadia-Version 4.01.1," NASA/TM-2009-215388, Oct. 2009.
[26] Gordon, S., and McBride, B. J., "Computer Program for Calculation of Complex Chemical Equilibrium Compositions and Applications, I: Analysis," NASA RP-1311, October 1994.
[27] Baldwin, B.S. and Lomax, H. "Thin Layer Approximation and Algebraic Model for Separated Turbulent Flows," AIAA Paper 78-0257. Huntsville, AL, 1978.
[28] Rizk, Y., "Prediction of Surface Roughness Effects on Hypersonic Turbulent Entry Heating," NASA/TM–215979, Sep. 27, 2012.
[29] Holman, J. P., *Experimental Methods for Engineers*, McGraw-Hill, 1984, Fourth Edition, p. 50.
[30] National Research Council Committee on the Planetary Science Decadal Survey, *Vision and Voyages for Planetary Science in the Decade 2013 -2022*, The National Academies Press, Washington, D.C., 2011.

(a) (b)

Figure 1. Ablated thermal protection material surface roughness examples: (a) Sand-grain-like roughness on the Stardust Mission sample return capsule; (b) Woven material (HEEET) roughness on an arcjet test sample.

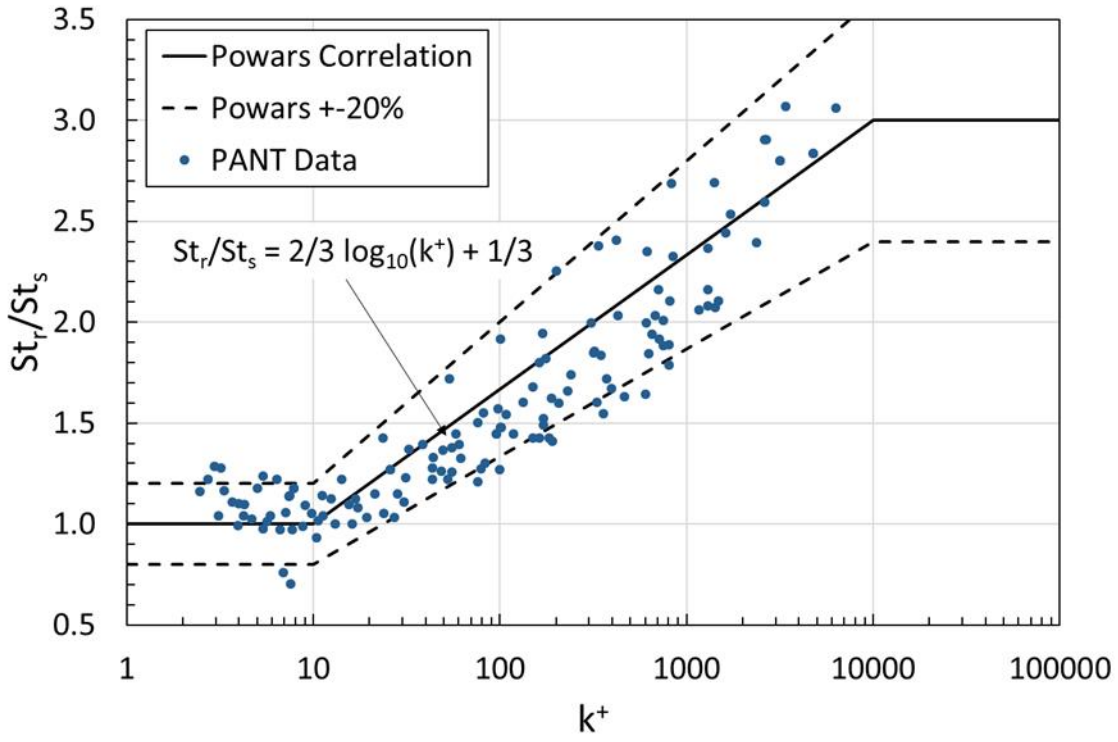

Figure 2. Powars' correlation of the effect on turbulent heat transfer of sand roughness, from the Passive Nosetip Technology (PANT) Program.

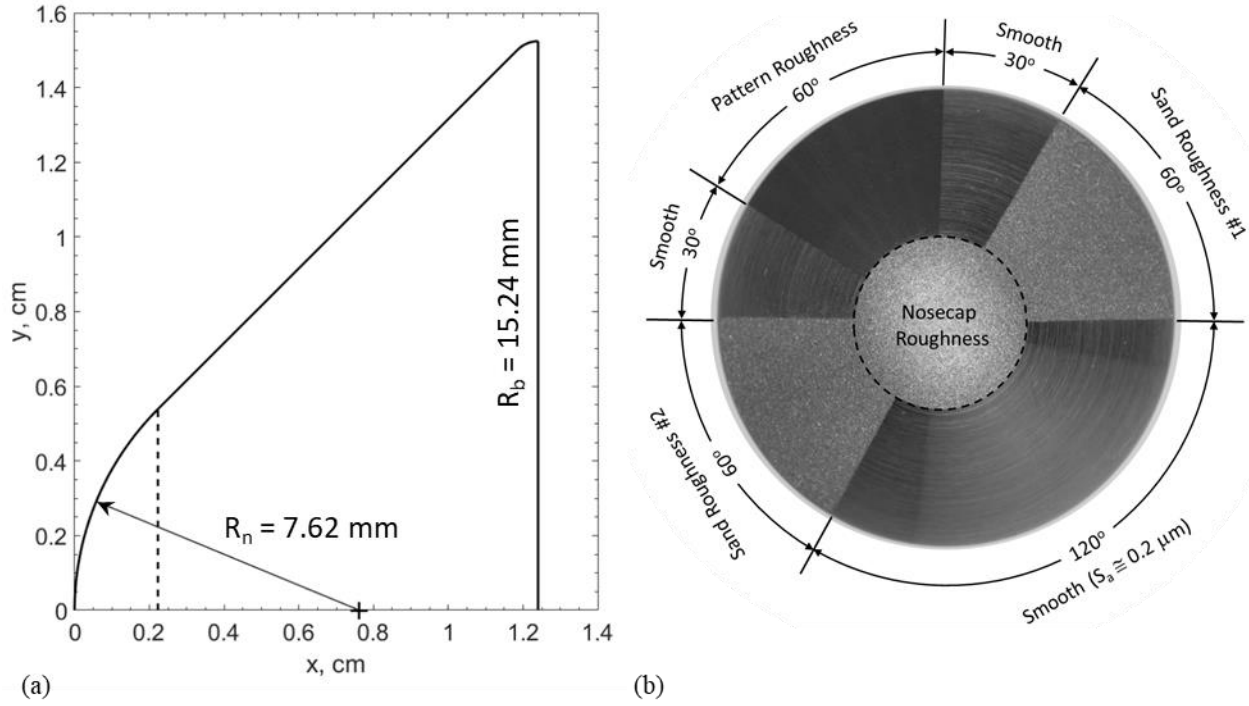

Figure 3. (a) Geometry of the ballistic range model, (b) top view of a model illustrating the layout of regions of various surface textures.

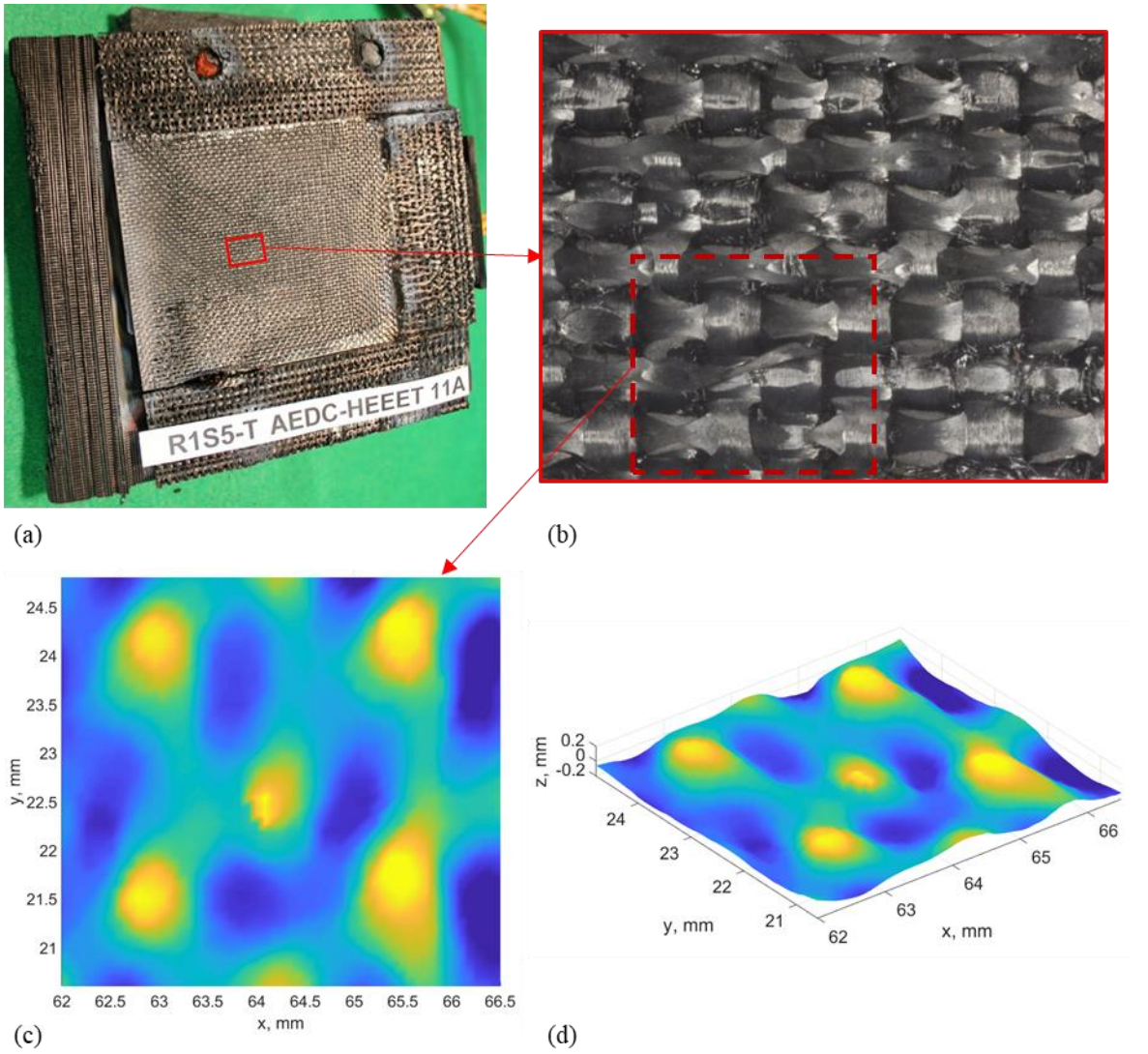

Figure 4. Woven TPS material pattern roughness: (a) Arcjet-ablated sample of HEEET material; (b) Close-up detail of (a); (c) and (d) 3D laser scan of surface pattern detail.

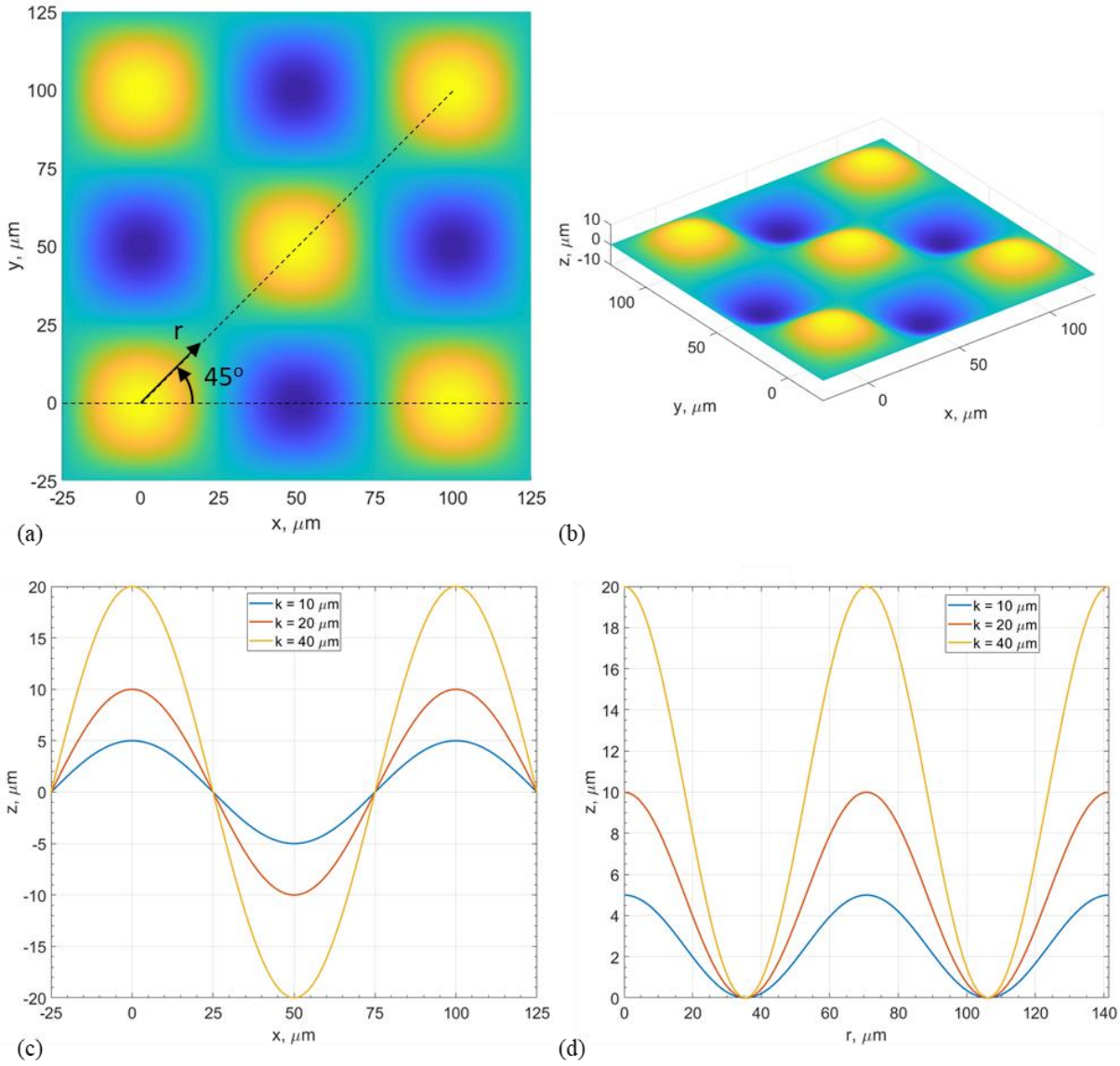

Figure 5. Idealized pattern roughness geometry: (a) basic pattern (k = 20 mm), top view; (b) oblique view, (c) axial profiles through two elements for each k; (d) diagonal profiles for each k.

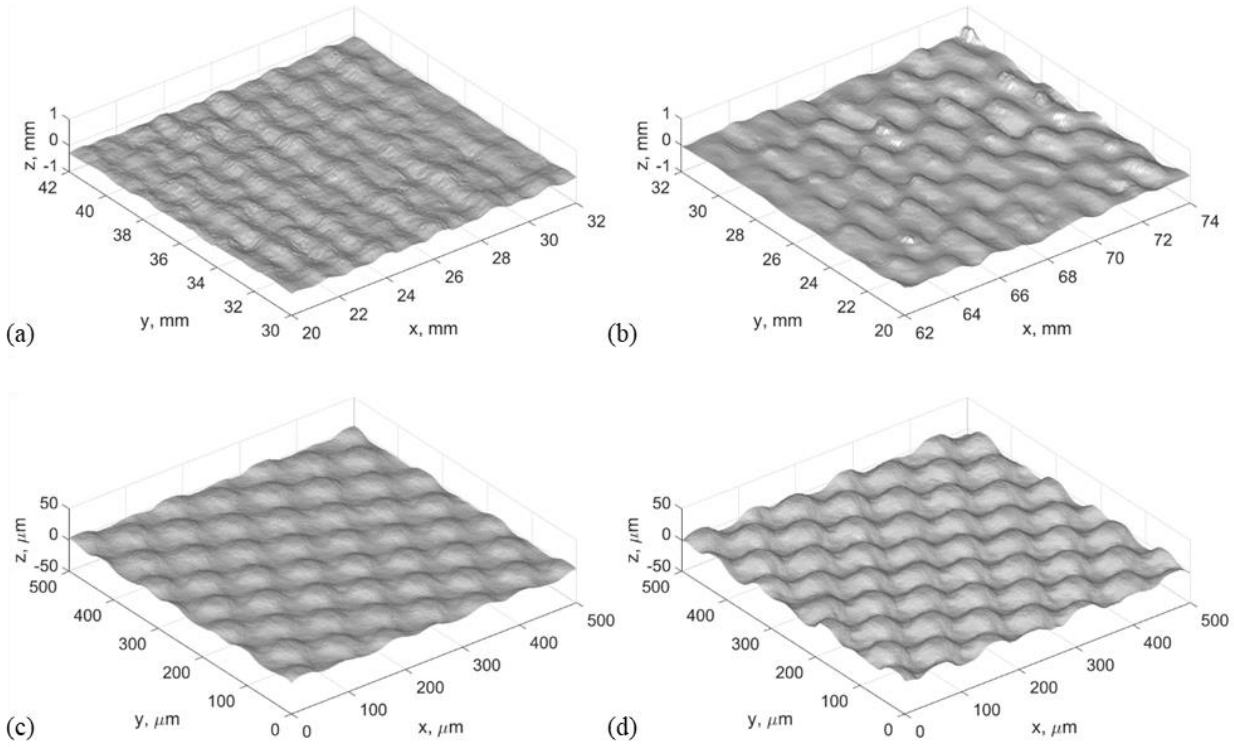

Figure 6. Surface scans of woven TPS materials compared with ballistic range models: (a) virgin TPS surface; (b) arcjet-ablated TPS surface; (c) area of model, k = 10 μm; (d) area of model, k = 20 μm.

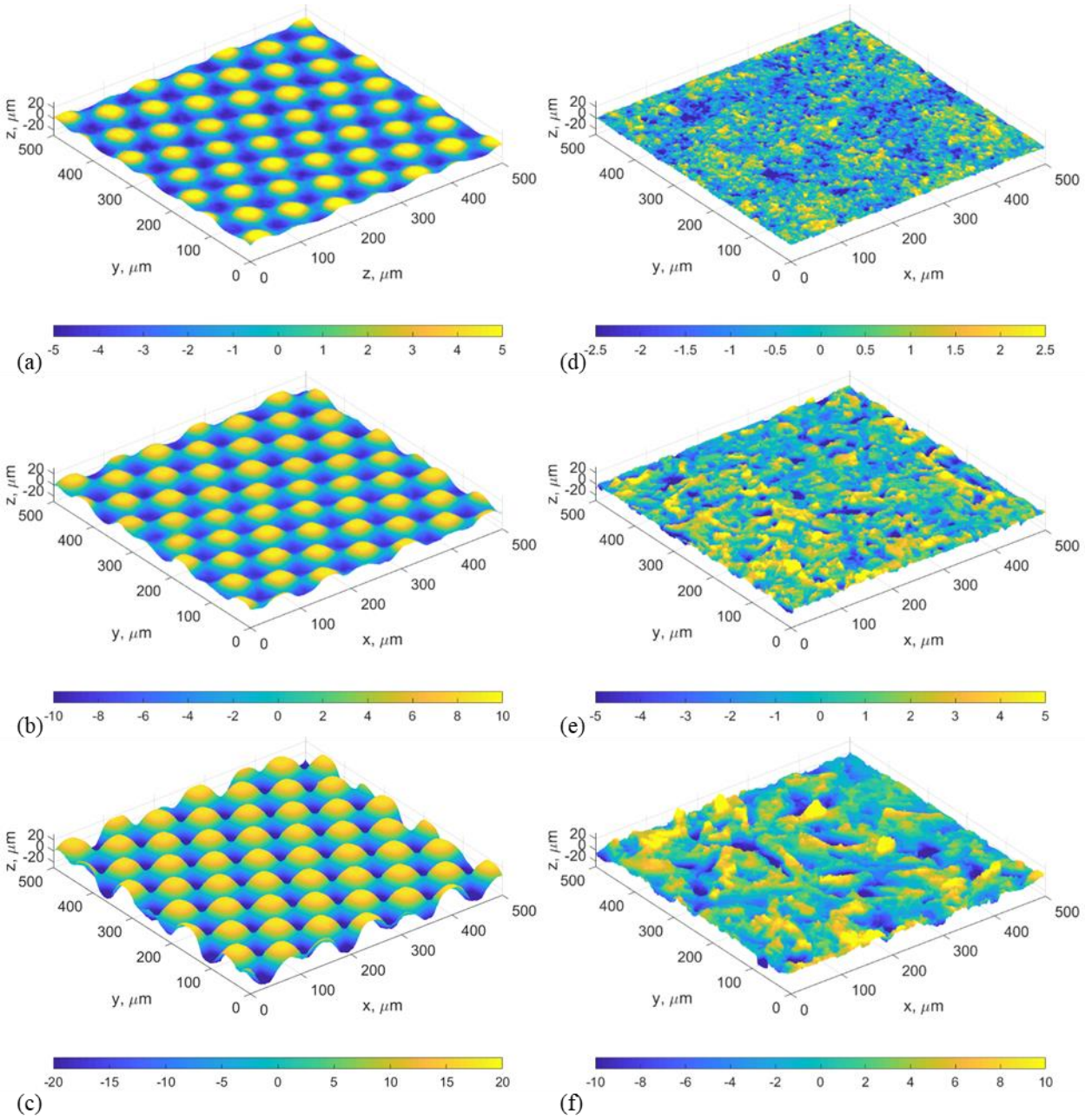

Figure 7. Representative surface scans of models: (a) pattern roughness, k = 10.5 mm, shot 2808, (b) pattern roughness, k = 19.7 mm, shot 2810, (c) pattern roughness, k = 42.6 mm, shot 2807, (d) sand roughness, k = 5.1 mm, shot 2808, (e) sand roughness, k = 11.4 mm, shot 2813, (f) sand roughness, k = 20.2 mm, shot 2810.

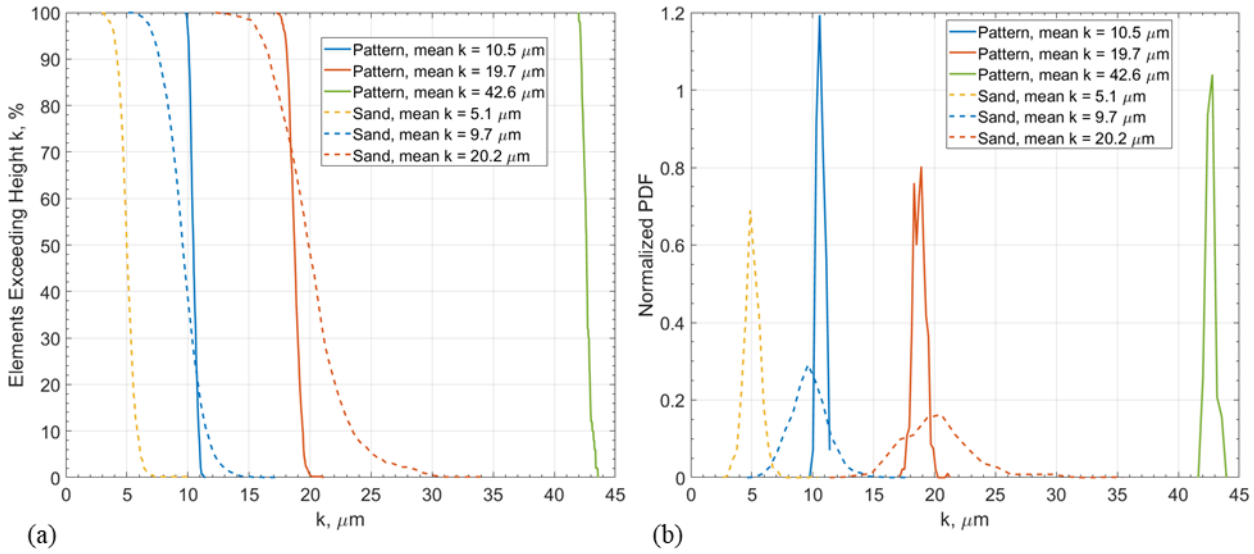

Figure 8. Characterization of the representative surfaces illustrating the distribution of roughness element sizes: (a) probability that any element exceeds height k, (b) probability distribution of element heights.

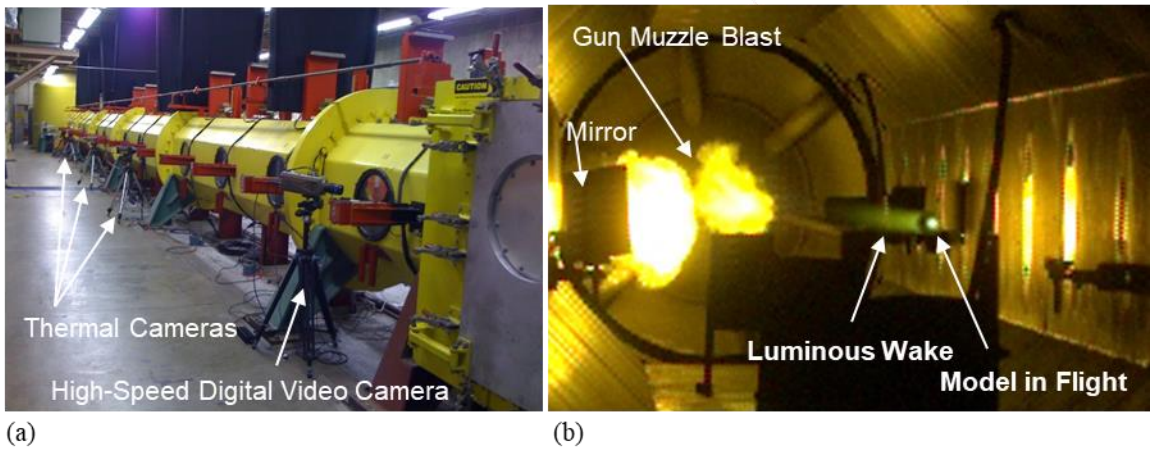

Figure 9. The Ames ballistic range test section: (a) external view; (b) internal view of model in flight.

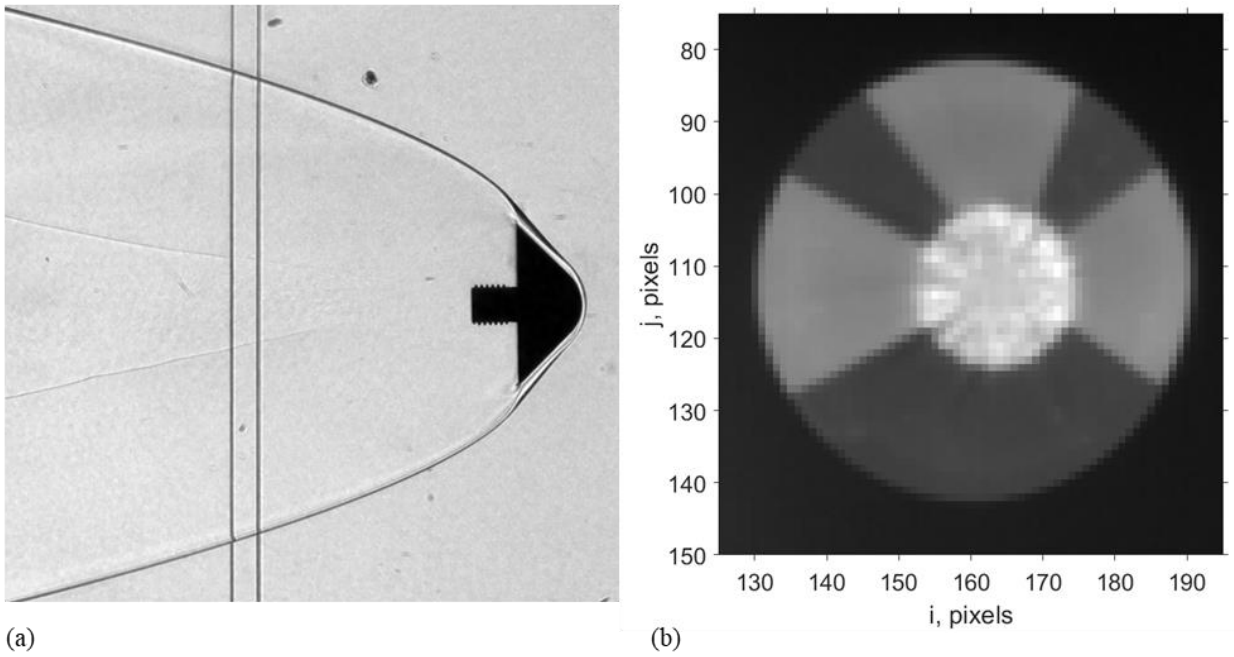

Figure 10. Images of a ballistic range model in flight: (a) shadowgraph image (side view); (b) mid-wave infrared image (front view).

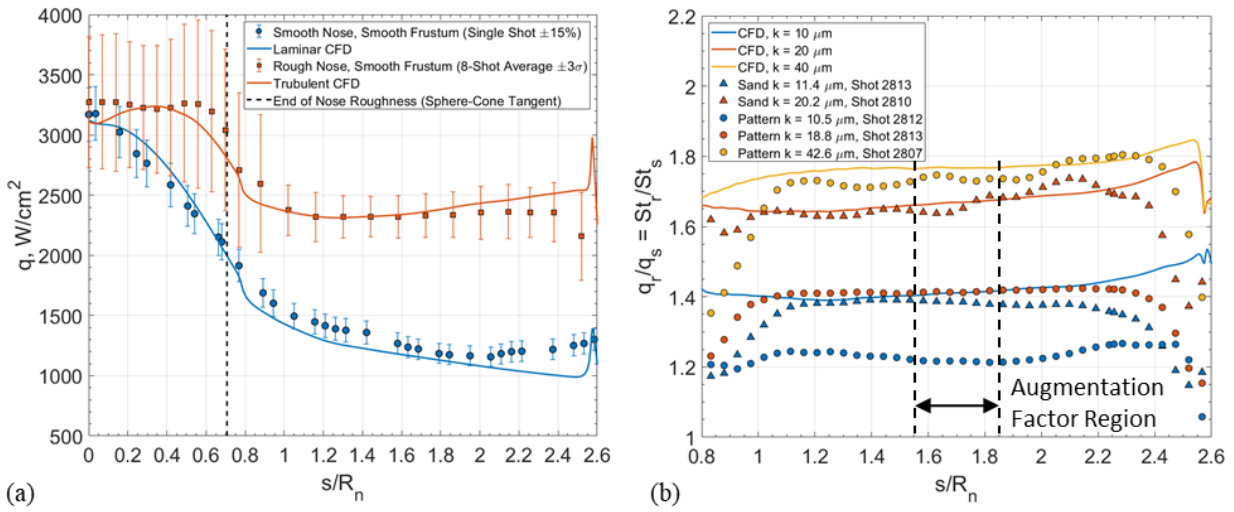

Figure 11. CFD solutions compared with representative measurements: (a) Smooth-wall, laminar and turbulent (experiment is tripped by 17 mm sand roughness on the nose cap); (b) Rough-wall turbulent frustum, shown as ratio of rough- to smooth-wall heat flux.

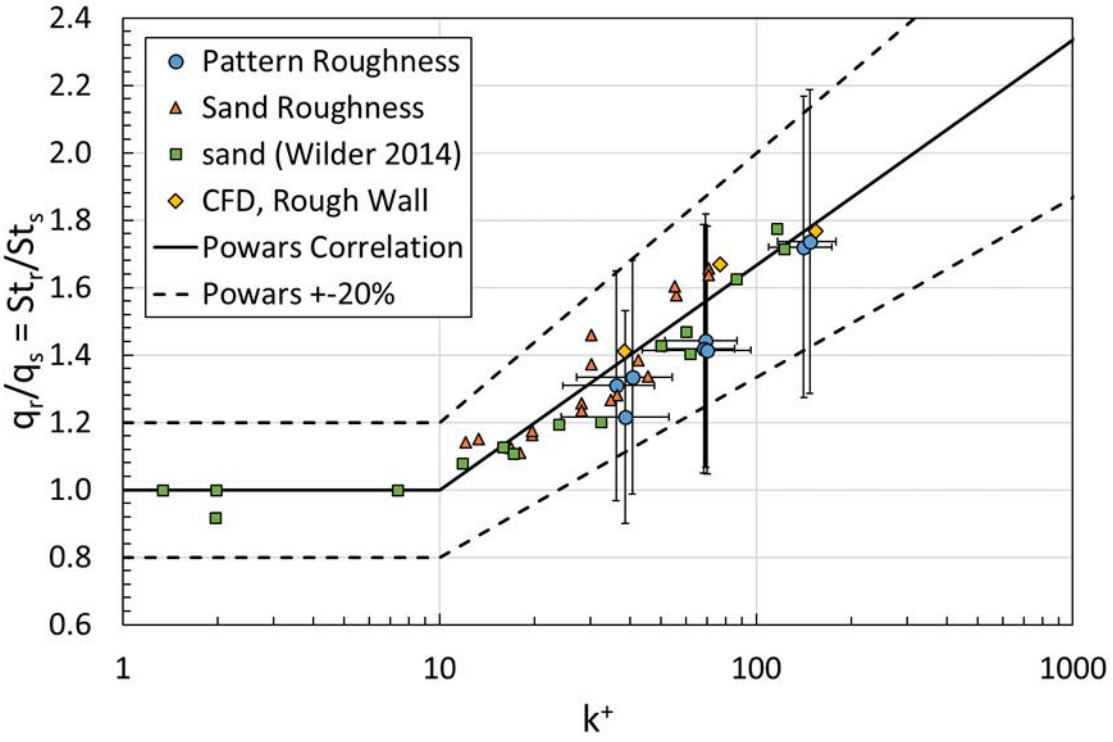

Figure 12. Rough-wall effect on turbulent heat transfer from the ballistic-range experiments of this paper, Wilder *et al.* 2014, and rough-wall CFD results. Pattern roughness k^+ is based on the actual k, rather than an equivalent sand grain roughness.

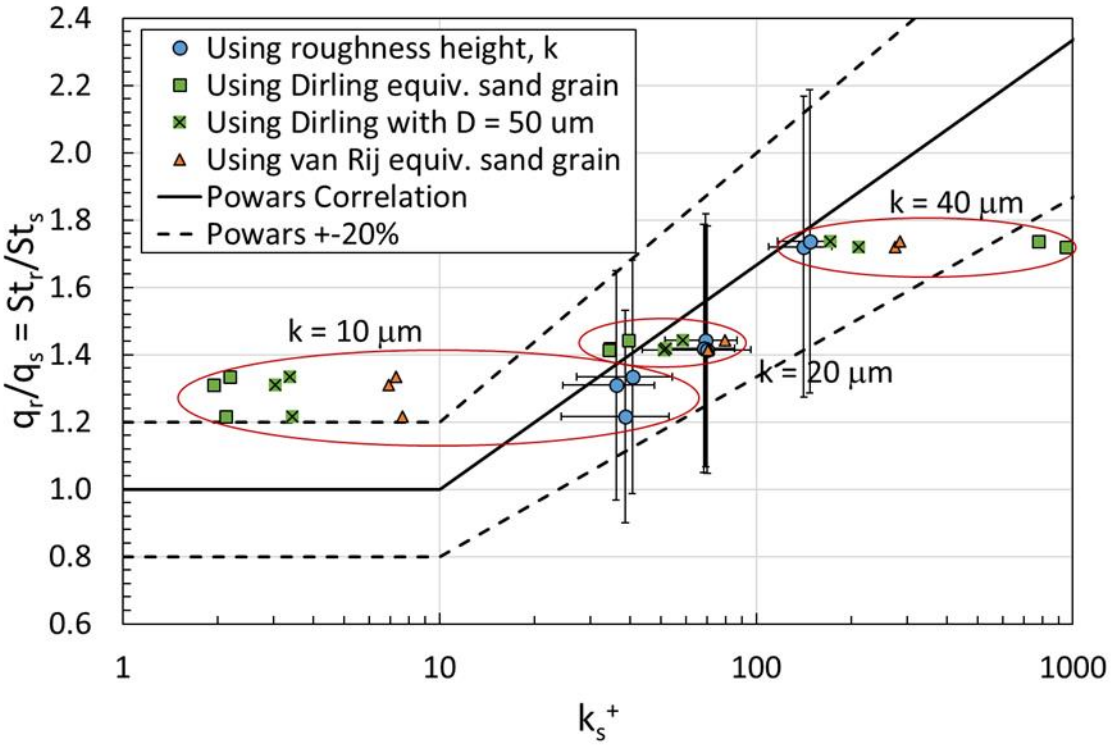

Figure 13. Rough-wall effect on turbulent heat transfer for pattern roughness, comparing ks+ based on two equivalent sand grain roughness correlations, and two interpretation of the roughness density for the Dirling shape parameter.

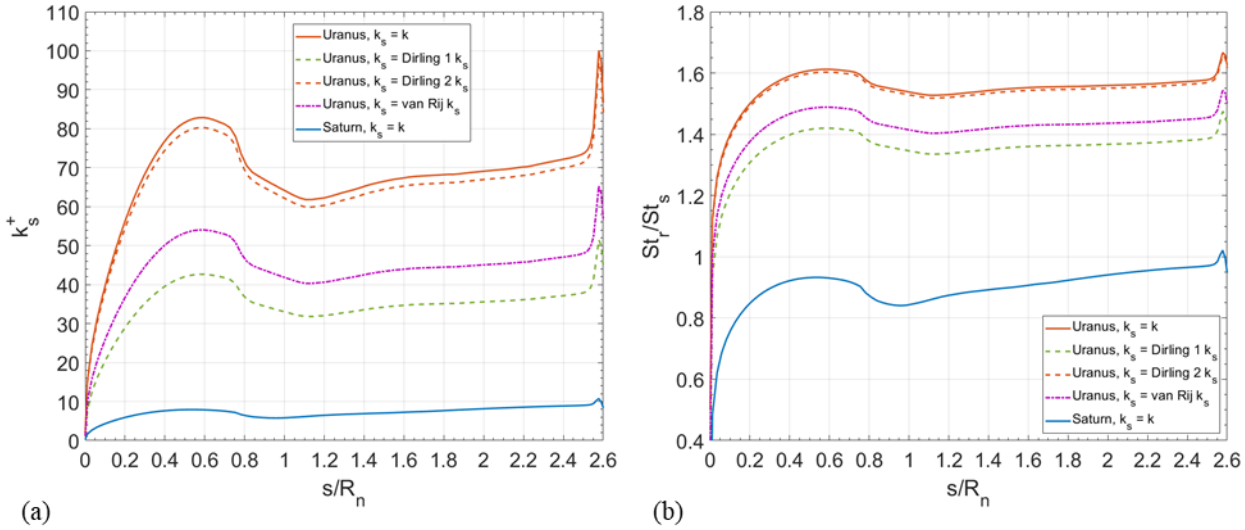

Figure 14. (a) Roughness Reynolds number distributions, and (b) turbulent convective heat transfer augmentation evaluated using Powars' correlation, on entry probes at Saturn and Uranus at the time of peak stagnation-point heat flux, for k = 0.74 mm.